Magnetic Chirality Controlled by the Interlayer Exchange Interaction

Mariëlle J. Meijer,[1,*] Juriaan Lucassen,[1] Fabian Kloodt-Twesten,[2] Robert Frömter,[2] Oleg Kurnosikov,[1] Rembert A. Duine,[1,3] Henk J. M. Swagten,[1] Bert Koopmans,[1] and Reinoud Lavrijsen[1]

[1]*Department of Applied Physics, Eindhoven University of Technology, P.O. Box 513, 5600 MB Eindhoven, Netherlands*
[2]*Universität Hamburg, Center for Hybrid Nanostructures, Luruper Chaussee 149, 22761 Hamburg, Germany*
[3]*Institute for Theoretical Physics, Utrecht University, Leuvenlaan 4, 3584 CE Utrecht, Netherlands*

(Received 30 October 2019; revised manuscript received 3 April 2020; accepted 27 April 2020; published 22 May 2020; corrected 23 July 2020)

Chiral magnetism, wherein there is a preferred sense of rotation of the magnetization, determines the chiral nature of magnetic textures such as skyrmions, domain walls, or spin spirals. Current research focuses on identifying and controlling the interactions that define the magnetic chirality in thin film multilayers. The influence of the interfacial Dzyaloshinskii-Moriya interaction (IDMI) and, recently, the dipolar interactions have been reported. Here, we experimentally demonstrate that an indirect interlayer exchange interaction can be used as an additional tool to effectively manipulate the magnetic chirality. We image the chirality of magnetic domain walls in a coupled bilayer system using scanning electron microscopy with polarization analysis. Upon increasing the interlayer exchange coupling, we induce a transition of the magnetic chirality from clockwise rotating Néel walls to degenerate Bloch-Néel domain walls and we confirm our findings with micromagnetic simulations. In multilayered systems relevant for skyrmion research, a uniform magnetic chirality across the magnetic layers is often desired. Additional simulations show that this can be achieved for reduced IDMI values (up to 30%) when exploiting the interlayer exchange interaction. This work opens up new ways to control and tailor the magnetic chirality by the interlayer exchange interaction.

DOI: 10.1103/PhysRevLett.124.207203

Magnetic chirality corresponds to a preferred sense of rotation of the magnetization and understanding this chirality has become of great importance for new spintronic applications [1–3]. These applications rely on the chiral nature of magnetic textures, like skyrmions or domain walls. In future magnetic memory devices, for instance, the racetrack memory [4], a controlled displacement of skyrmions or domain walls is of utmost importance for a reliable operation and a key requisite for this is a uniform magnetic chirality of the magnetic textures [5–9]. Current research focuses on identifying and controlling the interactions that define the magnetic chirality.

The most promising interaction that allows for the control of the magnetic chirality is the interfacial Dzyaloshinskii-Moriya interaction (IDMI), which has been studied extensively in the past years in magnetic thin films [10–13]. This interaction is an antisymmetric exchange interaction and originates from a broken symmetry at the interface of a ferromagnet and heavy metal [14–16]. The strength and sign of the IDMI depends on the specific material combination at an interface and the IDMI energetically favors either a clockwise (CW) or counterclockwise (CCW) rotation of the magnetization. This allows for the stabilization of magnetic textures, like skyrmions, Néel domain walls, or spin spirals, with a uniform magnetic chirality [1,15].

Very recently, it was recognized that dipolar fields also influence the magnetic chirality [17–22]. Although the effects of the dipolar interaction were already known for a long time [23–27], their impact on magnetic thin-film systems hosting an IDMI was only recently observed when stacking several magnetic thin films. These magnetic multilayers are commonly used to stabilize skyrmions at room temperature [9,28], and the increased magnetic volume leads to stronger dipolar fields. As a result, the dipolar field emitted from out-of-plane magnetized domains can influence the in-plane magnetization, which results in a nonuniform magnetic chirality across the magnetic multilayers. Various models [17–19] and first experiments [21] show that this behavior can be generalized and impacts other magnetic textures such as skyrmions. For most spintronic applications the stabilization of a uniform magnetic chirality across a multilayered system is desired, [17,19], which can be achieved by implementing a strong IDMI to overcome the dipolar interaction. Generating a strong IDMI is not always achievable, however, and severely constrains the design of the multilayered system.

In this Letter, we demonstrate an alternative approach to control the magnetic chirality utilizing the effect of an

indirect interlayer exchange interaction [29–33], namely the conventional Ruderman-Kittel-Kasuya-Yosida (RKKY) interaction [30,36,37] (the recently discovered asymmetric exchange component of the RKKY interaction is negligible in this work [34,35]). First, we determine the influence of the ferromagnetic (FM) RKKY interaction on the magnetic chirality by imaging the domain wall magnetization in a bilayer system with negligible IDMI using scanning electron microscopy with polarization analysis (SEMPA) [38–41]. In the absence of the RKKY interaction the dipolar fields cause a nonuniform magnetic chirality in the bilayer system with CW Néel walls in the top magnetic layer and CCW Néel walls in the bottom magnetic layer, as is schematically depicted in Fig. 1(a). Upon increasing the ferromagnetic RKKY coupling, the magnetization in the domain walls asymptotically rotates toward nonchiral Bloch walls. In the second part we investigate a multilayered system including IDMI typically used for skyrmion research with the help of micromagnetic simulations. We explicitly show that the necessary IDMI values to obtain a uniform magnetic chirality can be reduced by 30% in the presence of a strong ferromagnetic RKKY interaction. Utilizing the RKKY interaction therefore opens up new ways to tune and control the chirality of magnetic textures on a layer-by-layer basis.

Before we discuss our experimental results, we would like to first address how the dipolar fields and the ferromagnetic RKKY influence the magnetic chirality in the absence of an IDMI. Therefore, we concentrate on an elementary model consisting of two magnetic CoNi layers RKKY coupled via an Ir spacer layer as depicted in Fig. 1(a), which mimics the experimental situation. Both layers exhibit a perpendicular magnetic anisotropy and the up and down domains (white and black areas, respectively) of the magnetic bilayer generate dipolar fields as indicated by the gray dashed line. The in-plane magnetization direction inside the domain walls aligns with the dipolar fields as depicted by the arrows in the green and pink area and this leads to the formation of a CW Néel wall in the top magnetic layer and a CCW Néel wall in the bottom magnetic layer. By coupling the magnetic layers ferromagnetically (dashed blue line) this antiparallel alignment of the magnetization in the domain wall can be counteracted, resulting in the stabilization of degenerate Bloch walls pointing either into the paper (as indicated by the blue arrows) or out of the paper (not shown).

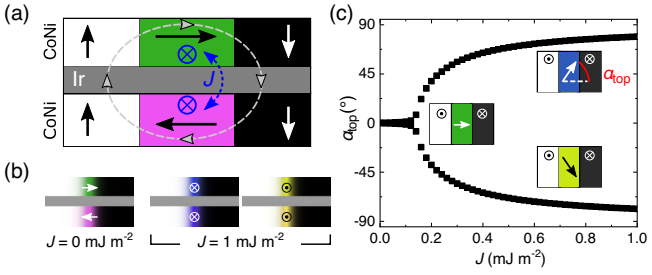

FIG. 1. (a) Elementary model of two magnetic CoNi layers separated by an Ir spacer layer in the absence of an IDMI (side view). The up and down domains are indicated by the white and black areas, respectively, and they generate dipolar fields (gray dashed lines). The in-plane magnetization of the domain wall aligns with the dipolar field (along the arrow), resulting in CW (CCW) Néel walls in the top (bottom) magnetic layer. A ferromagnetic RKKY interaction (blue dashed line) rotates the in-plane magnetization toward Bloch walls (blue arrows). (b) Micromagnetic simulation results for $J = 0$ mJ m^{-2} and the two degenerate cases for $J = 1$ mJ m^{-2}. The in-plane magnetization is indicated by the arrows. (c) Angle α_{top} as a function of RKKY coupling strength J obtained from micromagnetic simulations. α_{top} defines the angle between the in-plane magnetization and the horizontal of the top magnetic layer (see inset). The insets show a top view of the magnetization direction for $J = 0$ mJ m^{-2} (left-hand inset) and $J = 0.4$ mJ m^{-2} (right-hand insets for the degenerate case).

We confirm the validity of this intuitive picture using MuMax3 [42,43] micromagnetic simulations, with the simulation conditions specified in Supplemental Material SI [44]. On the left-hand side of Fig. 1(b) the result in the absence of a ferromagnetic RKKY coupling ($J = 0$ mJ m^{-2}) is depicted and the formation of a CW (CCW) Néel wall in the top (bottom) magnetic layer is found, respectively, as expected from the dipolar interaction. Introducing a ferromagnetic RKKY coupling ($J = 1$ mJ m^{-2}) leads to the formation of two energetically degenerate Bloch walls, as depicted on the right-hand side of Fig. 1(b), where the in-plane magnetization direction of both magnetic layers points either into the paper (blue area) or out of the paper (yellow area). We therefore find that a uniform magnetization profile across the magnetic layers in a bilayer system can be achieved due to the presence of a ferromagnetic RKKY interaction. A preferred chirality is not present, however, since two kinds of Bloch domain walls can be stabilized. In Fig. 1(c) we study the transition between Néel and Bloch walls as a function of J in more detail. Here, we focus on the domain wall formation in the top magnetic layer and the angle α_{top} describes the in-plane magnetization direction of the domain wall as depicted schematically in the top right-hand inset. We find that $\alpha_{top} = 0°$ for $J = 0$ mJ m^{-2} (see left-hand inset) and α_{top} asymptotically approaches the formation of Bloch walls ($\alpha_{top} = \pm 90°$) for large J. For intermediate values of J degenerate Bloch-Néel domain walls are formed and this is schematically depicted in the insets on the right-hand side for a value of $J = 0.4$ mJ m^{-2}. The micromagnetic results indicate that the ferromagnetic RKKY interaction determines the in-plane magnetization direction of the domain walls.

In the following we experimentally measure this influence by imaging the domain wall chirality in a bilayer system with SEMPA for different RKKY coupling strengths. Here, we map the magnetization profile of

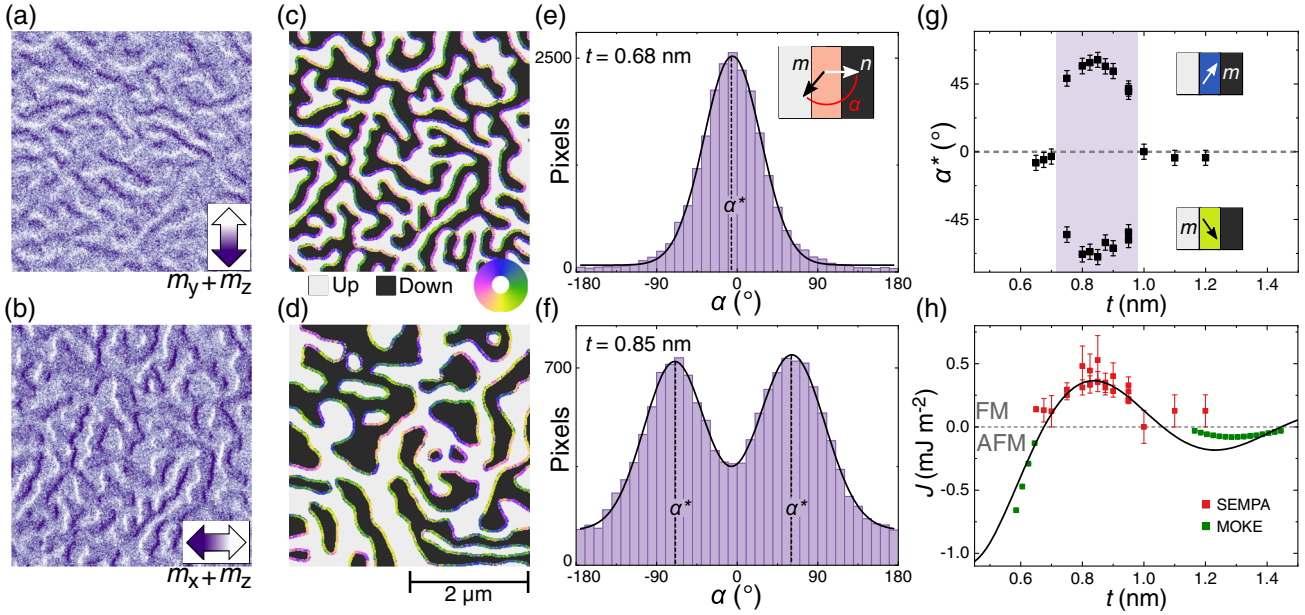

FIG. 2. (a),(b) SEMPA images of the top magnetic layer at an Ir thickness of $t = 0.68$ nm. Panel (a) shows m_y + out-of-plane contrast (m_z) and panel (b) m_x + out-of-plane contrast (m_z) for the same area. The in-plane magnetic contrast direction is indicated by the arrow in the bottom right-hand corner. (c) Composite image constructed from (a) and (b), with the in-plane magnetization indicated by the color wheel and the out-of-plane contrast by the white and black areas (up and down magnetization, respectively). (d) Composite image at an Ir thickness of $t = 0.85$ nm. The same scale bar is used for all images. (e),(f) Histograms of the angle α for all pixels in the domain walls of panels (c) and (d), respectively. α is defined as the difference between the domain wall normal n and magnetization in the domain wall m [see inset of (e)]. The solid line is a (double) Gaussian fit with the maximum(s) at α^*. (g) Maximum(s) α^* of the Gaussian fits of the histograms as a function of Ir thickness t. In the purple-shaded area two maximums are found and the insets schematically show the corresponding magnetization texture in this region. The color indications from (c) are used. (h) RKKY coupling strength J as a function of Ir spacer layer thickness t. The MOKE data are extracted from hysteresis loops (see Supplemental Material SIV for details [44]) and the SEMPA data in (g) are translated to a value of J with the help of Fig. 1(c). Both datasets are fitted with the theoretical RKKY function from Ref. [30] (solid black curve).

specifically the top magnetic layer, due to the high surface sensitivity of SEMPA. From literature it is known that iridium mediates a strong RKKY interaction that alternates between an antiferromagnetic (AFM) ($J < 0$) and ferromagnetic ($J > 0$) coupling as a function of thickness t with a damped sinusoidal behavior [29,30,36,37]. We therefore grew a sample with the following composition: //Ta(3)/Pt(3)/$[\mathrm{Co}(0.6)/\mathrm{Ni}(0.35)]_{x2}$Co(0.2)/Ir($t$)/$[\mathrm{Co}(0.6)/\mathrm{Ni}(0.35)]_{x2}$ (thicknesses in parentheses in nm), where the Ir thickness is wedged from $t = 0.5$–1.5 nm (see Supplemental Material SII for more details on the sample preparation [44]).

In Figs. 2(a) and 2(b) SEMPA images of the top magnetic layer are depicted at an Ir thickness of $t = 0.68$ nm. Figure 2(a) displays the m_y magnetization contrast and Fig. 2(b) the m_x magnetization contrast, as indicated by the arrows in the bottom right-hand corner. In both images a slight out-of-plane contrast is also visible (see Supplemental Material SII for details [44]), where the lighter areas correspond to up domains and the darker areas to down domains. The domains are framed by dark or light bands, which correspond to the in-plane component of the magnetization in the domain wall. The combined information of the SEMPA images is depicted in the composite image of Fig. 2(c) using a procedure described elsewhere [22]. Here, the out-of-plane contrast is indicated by the white and dark areas (up and down, respectively), and the in-plane magnetization direction in the domain wall is indicated by the color wheel. The coloring in the domain wall indicates that the magnetization always points from an up domain toward a down domain and reveals the presence of CW Néel walls. We can investigate this more thoroughly by defining an angle α, which is the difference between the domain wall normal n and the magnetization direction m, as depicted in the inset of Fig. 2(e). Assigning this angle α to every pixel in the domain wall results in the histogram shown in Fig. 2(e). Around $\alpha = 0°$ a peak in the histogram is observed that corresponds to the formation of CW Néel walls. The histogram is fitted with a Gaussian curve that models the underlying statistics of the individual pixels [22] and allows one to extract the peak position α^*. For an Ir thickness of $t = 0.85$ nm the same procedure results in the composite image shown in Fig. 2(d), and the corresponding histogram is depicted in Fig. 2(f). In the histogram two distinct peaks are observed and their position is extracted with a double Gaussian fit giving $\alpha^* = -70° \pm 5°$ and $\alpha^* = 61° \pm 5°$. The two types of domain walls that are

stabilized in Figs. 2(d) and 2(f) are neither CW Néel walls ($\alpha^* = 0°$) nor Bloch walls ($\alpha^* = \pm 90°$), but show rather an intermediate Bloch-Néel texture, as is schematically depicted in the insets of Fig. 1(c). Additional measurements for different Ir thicknesses can be found in Supplemental Material SIII [44].

The extracted α^* is plotted as a function of Ir thickness t in Fig. 2(g). CW Néel walls are formed for $t < 0.75$ nm and $t > 1.0$ nm, and the two degenerate Bloch-Néel walls are present for intermediate Ir thicknesses in the purple-shaded area. According to the findings presented in Fig. 1(c), the CW Néel walls are stabilized by the dipolar interaction. The formation of the degenerate Bloch-Néel walls in the purple-shaded area can then be explained by the interplay between the dipolar interaction and ferromagnetic RKKY interaction.

To further substantiate that the interlayer exchange interaction is the dominant mechanism that stabilizes the degenerate Bloch-Néel walls, we study the expected oscillatory behavior of the RKKY interaction in more detail. Therefore, we combine the information on the coupling strength in both the ferromagnetic and antiferromagnetic region as a function of the Ir layer thickness t, and this is plotted in Fig. 2(h). The data in the ferromagnetic region are plotted in red and obtained via the SEMPA measurements discussed previously, where the angle α^* from Fig. 2(g) is converted to a coupling strength J using the micromagnetic simulations presented in Fig. 1(c). Information on the coupling strength in the antiferromagnetic RKKY region can be obtained from the switching fields in the antiferromagnetic hysteresis loops measured by the magneto-optical Kerr effect (MOKE), as is explained in more detail in Supplemental Material SIV [44]. In Fig. 2(h) the coupling values in the antiferromagnetic region are plotted in green. When we combine both datasets we clearly observe the oscillatory behavior of the RKKY coupling J as a function of the Ir thickness t and the data are fitted with the theoretically predicted RKKY behavior [30] (solid black curve). The theory describes the periodic behavior well, and a maximum ferromagnetic coupling of approximately 0.4 mJ m^{-2} is obtained at $t = 0.85$ nm. Both the extracted period of the oscillation as well as the RKKY coupling strength remain valid when considering an IDMI in the stack, as is discussed in Supplemental Material Sec. SV [44], and are in agreement with values found in literature [36,37,45].

So far, we have seen experimentally and from micromagnetic simulations that in the absence of an IDMI the RKKY interaction influences the magnetic chirality induced by the dipolar interaction. Moreover, the simulations of Fig. 1(b) indicate that for a strong coupling almost identical magnetic textures are stabilized in the top and bottom magnetic layer. A uniform magnetic chirality cannot be obtained by the ferromagnetic RKKY interaction alone, however, due to the degeneracy of the Bloch-(Néel) walls. Adding an IDMI can lift this degeneracy and a uniform chirality across the magnetic layers can be achieved.

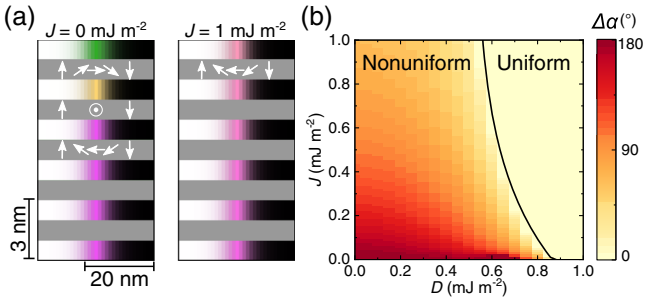

FIG. 3. (a) Micromagnetic simulations of a multilayer stack containing 6 magnetic layers with $D = 0.5$ mJ m^{-2}. The up and down domains are indicated by the white and black areas, respectively, and the colors in the domain walls show the in-plane magnetization direction according to the color wheel of Fig. 2(c). The arrows in the gray spacer layer indicate the magnetization inside the magnetic layer above. In the left-hand image $J = 0$ mJ m^{-2}, and in the right-hand image $J = 1$ mJ m^{-2}. (b) Phase diagram of the angle $\Delta\alpha$ as a function of J and D. $\Delta\alpha$ is defined as the difference between α in the bottom and top magnetic layer. For $\Delta\alpha = 0°$ there is a uniform chirality throughout the multilayer stack. The black line indicates from which D onward $\Delta\alpha < 0.1°$, marking the transition between a nonuniform and a uniform magnetization.

In the following we examine the necessary conditions to obtain a uniform magnetic chirality across the magnetic multilayers, when the dipolar interaction, RKKY interaction, and IDMI are present. We study this with micromagnetic simulations in a multilayered system typically hosting chiral magnetic textures like skyrmions. The investigated multilayered stack consists of 6 repeats with alternating magnetic and spacer layers of 1 nm (details of the simulations and the dependence on saturation magnetization M_S and effective anisotropy K_{eff} values can be found in the Supplemental Material SI and SVI [44]). In Fig. 3(a) the magnetic textures obtained for two RKKY strengths are depicted with an IDMI of $D = 0.5$ mJ m^{-2}. In the left-hand image $J = 0$ mJ m^{-2} and a nonuniform magnetization texture is observed across the magnetic layers. The bottom layers form CCW Néel walls, favored by the positive D, but the IDMI is not strong enough to counteract the dipolar interaction. This results in the formation of a Bloch wall and CW Néel wall in the top two layers. We define the uniformity of the chirality in the multilayered system by subtracting the α values from the bottom and top magnetic layer, and this results in $\Delta\alpha = 180°$ for the case of $J = 0$ mJ m^{-2}. In the right-hand image of Fig. 3(a) $J = 1$ mJ m^{-2} and an approximately uniform chirality in all the magnetic layers is achieved with $\Delta\alpha = 7°$. In Fig. 3(b) $\Delta\alpha$ is plotted for a range of D and J values. Two regions are indicated where the chirality is either nonuniform ($\Delta\alpha \neq 0°$) or uniform ($\Delta\alpha = 0°$). Without a RKKY

interaction ($J = 0$ mJ m^{-2}) an IDMI value of at least $D = 0.9$ mJ m^{-2} is needed to stabilize a uniform chirality, and this corresponds to the critical IDMI value of the system. Interestingly, this critical IDMI value can be reduced by approximately 30% when a RKKY interaction of $J = 1$ mJ m^{-2} is present, as can be seen from the transition line in Fig. 3(b). In practice these D and J values can be achieved in magnetic multilayers by optimizing the thicknesses and materials of the magnetic and nonmagnetic spacer layer [10,36], which makes it possible to stabilize magnetic textures with a uniform chirality in a wider variety of multilayered systems than previously assumed.

Finally, an additional effect of the interlayer exchange coupling on the magnetic texture becomes apparent when we compare the images of Figs. 2(c) and 2(d). The average domain size grows as the ferromagnetic RKKY interaction increases, and this is elaborated in more detail in Supplemental Material SVII [44]. Although the influence of the IDMI is not considered yet, the findings suggest that the RKKY interaction might be used to control the size of magnetic domains and possibly even skyrmions. Moreover, the influence of the RKKY interaction on the domain size needs to be considered when extracting magnetic parameters from domain patterns [31,46–48].

To conclude, we have demonstrated that an interlayer exchange interaction influences the magnetic chirality. In a system where dipolar fields are present, the influence of the RKKY interaction manifests itself as a rotation of the magnetization in the top domain wall from a CW Néel to a degenerate Bloch-Néel wall. We confirm these findings by micromagnetic simulations. Furthermore, micromagnetic simulations predict that the RKKY interaction reduces the IDMI required to obtain a uniform magnetic chirality across a typical multilayer system for skyrmion research. Making use of the well-known interlayer exchange interaction opens up new ways to tune and control the magnetic chirality in multilayered systems for spintronic applications.

This work is part of the research program of the Foundation for Fundamental Research on Matter (FOM), which is part of the Netherlands Organisation for Scientific Research (NWO). We acknowledge financial support by the DFG within SFB 668. R. A. D. also acknowledges the support of the European Research Council.

*m.j.meijer@tue.nl

[1] A. Fert, N. Reyren, and V. Cros, Nat. Rev. Mater. **2**, 17031 (2017).
[2] K. Everschor-Sitte, J. Masell, R. M. Reeve, and M. Kläui, J. Appl. Phys. **124**, 240901 (2018).
[3] N. Nagaosa and Y. Tokura, Nat. Nanotechnol. **8**, 899 (2013).
[4] A. Fert, V. Cros, and J. Sampaio, Nat. Nanotechnol. **8**, 152 (2013).
[5] A. Thiaville, S. Rohart, É. Jué, V. Cros, and A. Fert, Europhys. Lett. **100**, 57002 (2012).
[6] S. Emori, U. Bauer, S.-M. Ahn, E. Martinez, and G. S. D. Beach, Nat. Mater. **12**, 611 (2013).
[7] K.-S. Ryu, L. Thomas, S.-H. Yang, and S. Parkin, Nat. Nanotechnol. **8**, 527 (2013).
[8] J. Sampaio, V. Cros, S. Rohart, A. Thiaville, and A. Fert, Nat. Nanotechnol. **8**, 839 (2013).
[9] S. Woo, K. Litzius, B. Krüger, M.-Y. Im, L. Caretta, K. Richter, M. Mann, A. Krone, R. M. Reeve, M. Weigand, P. Agrawal, I. Lemesh, M.-A. Mawass, P. Fischer, M. Kläui, and G. S. D. Beach, Nat. Mater. **15**, 501 (2016).
[10] D.-S. Han, N.-H. Kim, J.-S. Kim, Y. Yin, J.-W. Koo, J. Cho, S. Lee, M. Kläui, H. J. M. Swagten, B. Koopmans, and C.-Y. You, Nano Lett. **16**, 4438 (2016).
[11] H. Yang, O. Boulle, V. Cros, A. Fert, and M. Chshiev, Sci. Rep. **8** 12356, (2018).
[12] X. Ma, G. Yu, C. Tang, X. Li, C. He, J. Shi, K. L. Wang, and X. Li, Phys. Rev. Lett. **120**, 157204 (2018).
[13] F. Kloodt-Twesten, S. Kuhrau, H. P. Oepen, and R. Frömter, Phys. Rev. B **100**, 100402(R) (2019).
[14] A. N. Bogdanov and U. K. Rößler, Phys. Rev. Lett. **87**, 037203 (2001).
[15] M. Bode, M. Heide, K. von Bergmann, P. Ferriani, S. Heinze, G. Bihlmayer, A. Kubetzka, O. Pietzsch, S. Blügel, and R. Wiesendanger, Nature (London) **447**, 190 (2007).
[16] M. Heide, G. Bihlmayer, and S. Blügel, Phys. Rev. B **78**, 140403(R) (2008).
[17] I. Lemesh and G. S. D. Beach, Phys. Rev. B **98**, 104402 (2018).
[18] W. Legrand, N. Ronceray, N. Reyren, D. Maccariello, V. Cros, and A. Fert, Phys. Rev. Applied **10**, 064042 (2018).
[19] W. Legrand, J.-Y. Chauleau, D. Maccariello, N. Reyren, S. Collin, K. Bouzehouane, N. Jaouen, V. Cros, and A. Fert, Sci. Adv. **4** eaat0415, (2018).
[20] K. Fallon, S. McVitie, W. Legrand, F. Ajejas, D. Maccariello, S. Collin, V. Cros, and N. Reyren, Phys. Rev. B **100**, 214431 (2019).
[21] Y. Dovzhenko, F. Casola, S. Schlotter, T. X. Zhou, F. Büttner, R. L. Walsworth, G. S. D. Beach, and A. Yacoby, Nat. Commun. **9**, 2712 (2018).
[22] J. Lucassen, M. J. Meijer, F. Kloodt-Twesten, R. Fromter, O. Kurnosikov, R. A. Duine, H. J. M. Swagten, B. Koopmans, and R. Lavrijsen, Phys. Rev. Lett. **123**, 157201 (2019).
[23] A. Hubert and R. Schäfer, *Magnetic Domains: The Analysis of Magnetic Microstructures*, 1st ed. (Springer-Verlag, Berlin, 1998), pp. 240–241.
[24] A. Malozemoff and J. Slonczewski, *Magnetic Domain Walls in Bubble Materials*, Applied Solid State Science: Supplement (Academic Press, New York, 1979).
[25] V. Kamberský, J. Magn. Soc. Jpn. **19**, S1_37 (1995).
[26] M. Labrune and L. Belliard, Phys. Status Solidi A **174**, 483 (1999).
[27] M. Tekielak, R. Gieniusz, M. Kisielewski, P. Mazalski, A. Maziewski, V. Zablotskii, F. Stobiecki, B. Szymański, and R. Schäfer, J. Appl. Phys. **110**, 043924 (2011).
[28] C. Moreau-Luchaire, C. Moutafis, N. Reyren, J. Sampaio, C. A. F. Vaz, N. Van Horne, K. Bouzehouane, K. Garcia, C. Deranlot, P. Warnicke, P. Wohlhüter, J.-M. George, M.

Weigand, J. Raabe, V. Cros, and A. Fert, Nat. Nanotechnol. **11**, 444 (2016).
[29] M. Stiles, J. Magn. Magn. Mater. **200**, 322 (1999).
[30] P. Bruno, Phys. Rev. B **52**, 411 (1995).
[31] O. Hellwig, A. Berger, J. B. Kortright, and E. E. Fullerton, J. Magn. Magn. Mater. **319**, 13 (2007).
[32] G. Chen, A. Mascaraque, A. T. N'Diaye, and A. K. Schmid, Appl. Phys. Lett. **106**, 242404 (2015).
[33] A. K. Nandy, N. S. Kiselev, and S. Blügel, Phys. Rev. Lett. **116**, 177202 (2016).
[34] A. Fernández-Pacheco, E. Vedmedenko, F. Ummelen, R. Mansell, D. Petit, and R. P. Cowburn, Nat. Mater. **18**, 679 (2019).
[35] D.-S. Han, K. Lee, J.-P. Hanke, Y. Mokrousov, K.-W. Kim, W. Yoo, Y. L. W. van Hees, T.-W. Kim, R. Lavrijsen, C.-Y. You, H. J. M. Swagten, M.-H. Jung, and M. Kläui, Nat. Mater. **18**, 703 (2019).
[36] S. S. P. Parkin, Phys. Rev. Lett. **67**, 3598 (1991).
[37] Y. Luo, M. Moske, and K. Samwer, Europhys. Lett. **42**, 565 (1998).
[38] H. Oepen and H. Hopster, SEMPA studies of thin films, structures, and exchange coupled layers, in *Magnetic Microscopy of Nanostructures*, edited by H. Hopster and H. P. Oepen (Springer, Berlin, 2005), pp. 137–167.
[39] J. Unguris, Scanning electron microscopy with polarization analysis (SEMPA) and its applications, in *Experimental Methods in the Physical Sciences*, Vol. 36, edited by M. De Graef and Y. Zhu (Academic Press, San Diego, 2001), pp. 167–193.
[40] R. Frömter, S. Hankemeier, H. P. Oepen, and J. Kirschner, Rev. Sci. Instrum. **82**, 033704 (2011).
[41] E. C. Corredor, S. Kuhrau, F. Kloodt-Twesten, R. Frömter, and H. P. Oepen, Phys. Rev. B **96**, 060410(R) (2017).
[42] A. Vansteenkiste, J. Leliaert, M. Dvornik, M. Helsen, F. Garcia-Sanchez, and B. Van Waeyenberge, AIP Adv. **4**, 107133 (2014).
[43] J. D. Clercq, J. Leliaert, and B. V. Waeyenberge, J. Phys. D **50**, 425002 (2017).
[44] See Supplemental Material at http://link.aps.org/supplemental/10.1103/PhysRevLett.124.207203 for (I) details on micromagnetic simulations, (II) details on the sample preparation and SEMPA, (III) supporting measurements, (IV) measuring the AF RKKY interaction, (V) dependence of in-plane magnetization on J and D, (VI) dependence of the uniform chirality on magnetic parameters and (VII) dependence of the domain size on J.
[45] S. Karayev, P. D. Murray, D. Khadka, T. R. Thapaliya, K. Liu, and S. X. Huang, Phys. Rev. Mater. **3**, 041401 (2019).
[46] H. Draaisma and W. De Jonge, J. Appl. Phys. **62**, 3318 (1987).
[47] I. Lemesh, F. Büttner, and G. S. D. Beach, Phys. Rev. B **95**, 174423 (2017).
[48] T. N. G. Meier, M. Kronseder, and C. H. Back, Phys. Rev. B **96**, 144408 (2017).

Correction: The use of the grouped byline format resulted in an incorrect author order, which has been rectified.